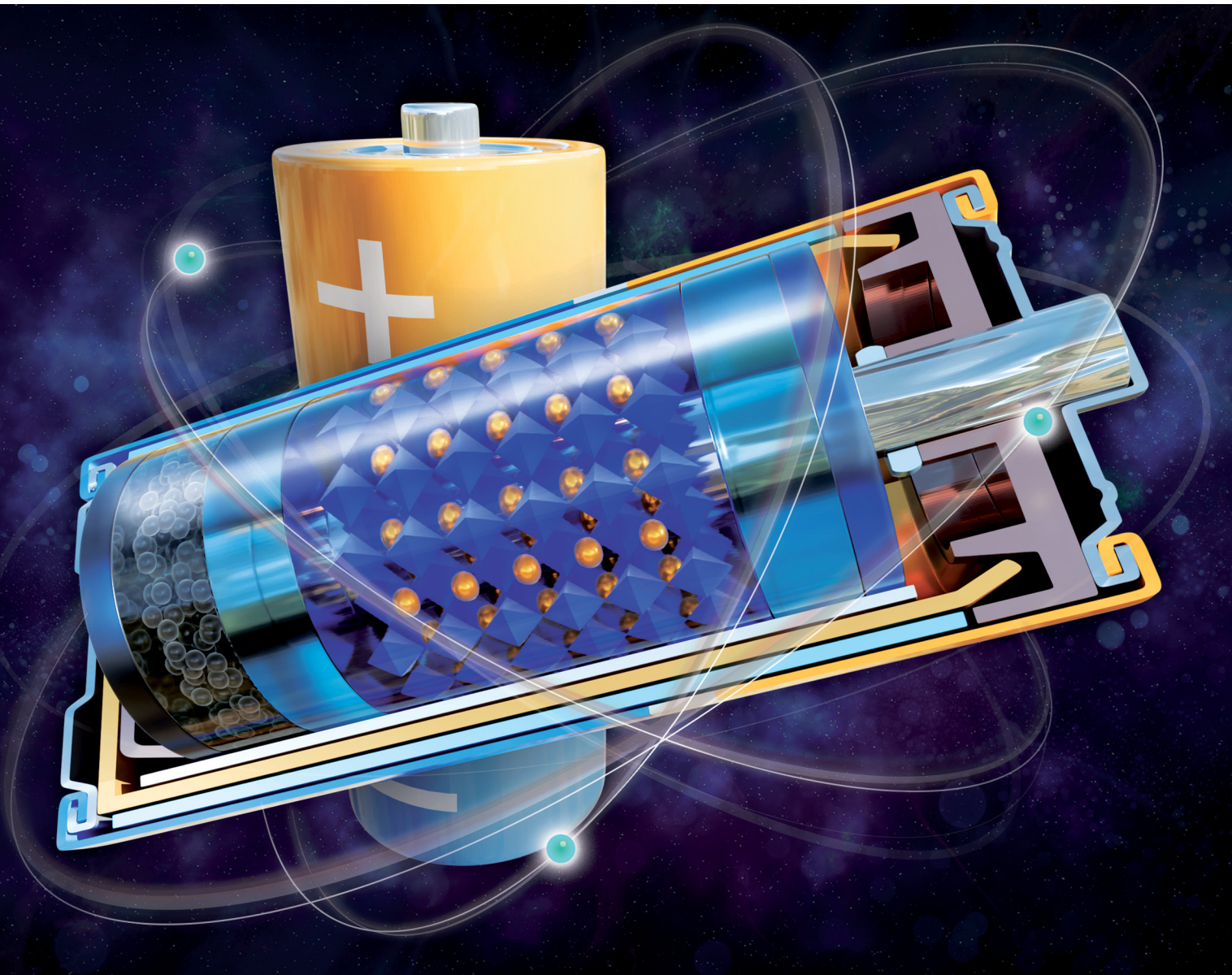


ChemComm

Chemical Communications

rsc.li/chemcomm



ISSN 1359-7345

COMMUNICATION

Su-Il In *et al.*

Novel perovskite-based betavoltaic cell: dual additive strategy for enhanced FAPbI_3 α -phase stability and performance



Cite this: *Chem. Commun.*, 2025, 61, 5930

Received 8th November 2024,
Accepted 25th February 2025

DOI: 10.1039/d4cc05935b

rsc.li/chemcomm

Novel perovskite-based betavoltaic cell: dual additive strategy for enhanced FAPbI_3 α -phase stability and performance[†]

Chol Hyun Kim,[‡] Muhammad Bilal Naseem,[‡] Junho Lee,[‡] Hong Soo Kim,[‡] Sanghun Lee and Su-Il In^{‡*}

By utilizing chlorine-based dual additives with perovskite film and radioactive isotopes of carbon nanoparticle/quantum dot ($^{14}\text{CNP}/\text{CQD}$) electrodes, we enhanced the phase stability and power conversion efficiency (PCE) of the betavoltaic device. This study represents the first successful integration of perovskite into a betavoltaic cell, pioneering perovskite betavoltaic cells (PBCs).

In recent years, the development of long-lasting and efficient energy sources to meet the changing energy requirements has become a matter of importance.^{1–3} Betavoltaic cells have emerged as a promising solution due to their ability to utilize radioisotopes as their energy source. They stand out for their remarkable longevity and high energy density, making them ideal for powering devices in remote or harsh environments where replacement or maintenance of the device is impractical. Betavoltaic cells convert incoming radiation energy into electrical power using a beta-radiation (β -radiation) absorption material. Betavoltaic devices mainly consist of a radioactive isotope as the energy source, a β -radiation absorbing material for energy conversion, and a counter electrode.^{4,5} The β -radiation absorbing material plays a critical role in converting radiation energy into electrical energy, directly influencing the cell's efficiency and stability.^{6–8} Considerable research on such materials has focused on semiconductors consisting of p-n junctions and Schottky barriers, however, the overall performance of betavoltaic cells still requires improvement for practical application.⁹ The energy conversion efficiency (ECE) of these devices is currently below 4%, and they have a maximum output power under 500 μW .^{10,11} To enhance β -radiation absorption, new material strategies are needed.

For this purpose, advanced materials that can better absorb β -radiation and efficiently convert it into electrical energy are

being researched.¹⁰ For such applications, organic–inorganic hybrid halide perovskites have garnered significant attention. These materials are known for their versatility and high electron–hole mobility and have a unique ABX_3 ionic crystal structure, where A is a cation, B is a metal, and X is a halide anion. Their tunable band gap, ranging from 1.5 to 3.3 eV, positions them as an exciting candidate for betavoltaic cells.^{12,13}

Recent advancements suggest that perovskites in betavoltaic cells could yield an ECE of up to 28%, a significant improvement compared to other materials.¹⁴ The interaction between beta-electrons (β -electrons) and the heavy atoms (such as Br, I, and Pb) found in perovskites enhances performance by shortening the penetration depth of beta-particles (β -particles), allowing for more efficient use of the β -radiation energy.^{15,16} Additionally, perovskites demonstrate impressive radiation resistance, withstanding high radiation thresholds of up to $1.35 \times 10^5 \text{ Ci cm}^{-2} \text{ s}^{-1}$ for extended periods (303 s).¹⁷ This aspect makes them well-suited for environments with high radiation exposure.

Despite these advantages, PBCs face several challenges related to achieving high efficiency and long-term stability. Their sensitivity to moisture and oxygen leads to degradation and phase transitions that compromise efficiency and long-term stability.¹⁸ Additionally, factors such as the presence of defects, trap states and the thickness of the perovskite film can impact the ECE of the device due to non-radiative recombination losses along with self-absorption and shielding effects, respectively. To address these issues, we introduce dual additives of MACl and CsCl into the perovskite material.¹⁹

Our strategy involves using methylammonium chloride (MACl) as an additive, which has demonstrated effectiveness in improving perovskite efficiency.²⁰ This approach has shown great potential in creating large perovskite domains, leading to large single-crystal grains with fewer defects and higher efficiency. However, the volatile nature of MACl poses stability concerns, as the methylammonium (MA) cation can cause degradation over time.^{21,22} As such, Cesium chloride (CsCl) is suggested as a potential candidate for improving the long-term stability of the perovskite. The cesium (Cs) cation is known to stabilize the crystal structure and enhance phase purity

Department of Energy Science & Engineering, Daegu Gyeongbuk Institute of Science & Technology (DGIST), 333 Techno Jungang-daero, Hyeonpung-eup, Dalseong-Gun, Daegu 42988, Republic of Korea. E-mail: insuil@dgist.ac.kr

[†] Electronic supplementary information (ESI) available. See DOI: <https://doi.org/10.1039/d4cc05935b>

[‡] These authors contributed equally.



when incorporated into FAPbI_3 perovskite lattices.²³ However, when used as an additive on its own, it lowers the photovoltaic performance of FAPbI_3 .¹⁹

Utilizing both MACl and CsCl as dual additives in the perovskite material has been shown to emphasize the benefits of both materials.

The introduction of CsCl significantly improves crystallinity, reduces trap density, and enhances both operational and environmental stability. The result is a high-efficiency, stable perovskite structure that outperforms systems using MACl alone.¹⁹

In this study, we explore the potential of this dual additive strategy to enhance the performance and stability of FAPbI_3 -based PBCs. By simultaneously utilizing both MACl and CsCl , we aim to create a more stable and efficient perovskite as β -radiation absorbing material, as depicted in Fig. 1. The stabilized structure of the FAPbI_3 perovskite was confirmed through scanning electron microscopy (SEM), X-ray photoelectron spectroscopy (XPS), and photoluminescence (PL) measurements. Our results indicate that this dual additive strategy not only improves the performance of the perovskite absorber in PBCs but also extends its operational stability. A critical factor affecting the performance of perovskite betavoltaic cells is the grain size and phase transition properties of the perovskite material. These parameters directly influence the density and diffusion coefficient of mobile ions, as well as the defect passivation of the material.^{14,24,25} To better understand these factors, we conducted an SEM analysis of the surface of the perovskite films (Fig. S1, ESI†). The thickness of the perovskite film is another crucial factor that must be controlled to reduce self-absorption and shielding effects.^{10,14} As shown in Fig. S2 (ESI†), the optimal thicknesses for the FAPbI_3 -based perovskite and Spiro-MeOTAD layers were found to be 500 nm and 200 nm, respectively. These dimensions correspond to the optimal thicknesses for maximizing electron-hole pair generation from incoming β -electrons.

To further understand the effects of the dual additive strategy, we performed X-ray diffraction (XRD) analysis to examine the phase transition properties of the films (Fig. 2A). The results show that the combined use of MACl and CsCl not only enhances grain size and crystallinity but also stabilizes the perovskite's crystal phase, making it a more efficient absorber for use in betavoltaic cells.

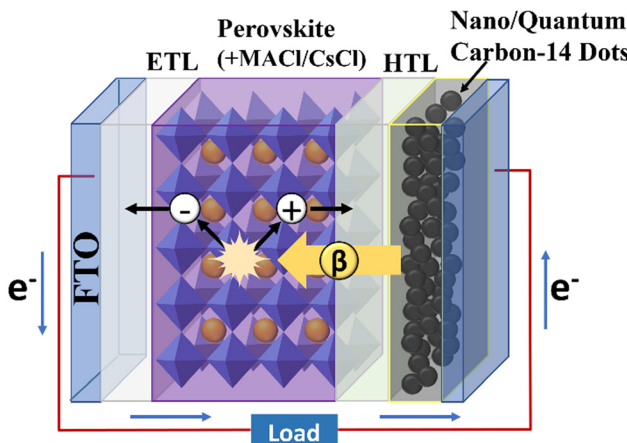


Fig. 1 Schematic mechanism illustration of the perovskite betavoltaic cell.

The XRD peaks are divided into an alpha (α)-phase at 14.0° , 19.9° , 24.4° , 28.2° , 31.6° , 34.8° , and 40.3° , except for the four characteristic peaks of the FTO substrate at 27.3° , 34.3° , 38.4° , and 43.3° .^{20,26}

Notably, there exists a trace amount of PbI_2 (12.9°) in single and dual additive samples, implying that Cl affects the nucleation and growth dynamics of perovskite films.²⁷ A small amount of PbI_2 has been considered favorable for device performance due to the passivation of interfacial traps, further supporting the optimization of perovskite materials for high efficiency.^{28–30} Compared to the FAPbI_3 without additives, the sharp and intensive peaks in MACl - and MACl/CsCl - FAPbI_3 plots imply that the films are well-crystallized, showcasing the superior structural integrity of perovskite films with dual additives. This high degree of crystallinity directly correlates with the enhanced electronic properties and stability discussed earlier.

The XRD peaks assigned to (001) and (002) crystal planes of the MACl - and MACl/CsCl - FAPbI_3 are slightly shifted to higher angles, indicating that the crystal lattices of FAPbI_3 perovskite shrink according to Bragg's law. This shrinkage reflects the successful incorporation of MA^+ and Cs^+ into the perovskite lattice, which reduces lattice distortion and defects. As noted earlier, this reduction in defects enhances carrier mobility, confirming that the dual additive approach optimizes the perovskite structure for efficient energy conversion.^{31,32} These findings align with the earlier assertion that the combination of MACl and CsCl improves phase purity and stability, crucial for long-term performance in betavoltaic cells.

From the SEM and XRD studies, it is evident that the dual additive strategy produces highly crystalline, large-grain perovskite films with a stable α -phase, as predicted. These characteristics are essential for achieving the high efficiency and operational stability mentioned earlier. Optoelectronic properties were confirmed using UV-vis and steady-state PL analyses to investigate the influence of additives on betavoltaic cell performance further. The UV-vis spectra (Fig. 2B) revealed a clear absorption shoulder in MACl - and MACl/CsCl - FAPbI_3 films around 800 nm, indicating excellent crystallinity.

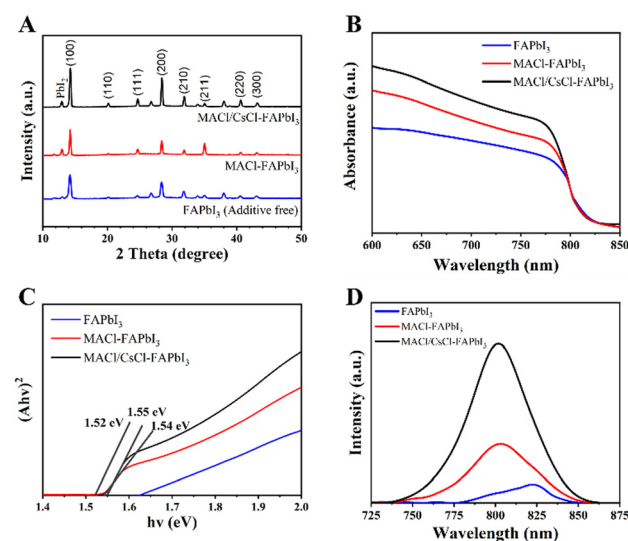


Fig. 2 (A) XRD patterns with perovskite films. Optoelectronic properties of perovskite films: (B) UV-vis, (C) Tauc plot, and (D) steady-state PL.

These results suggest that the dual additive method produces high-quality films with enhanced optical properties as claimed.

The optical bandgap, estimated from the Tauc plot (Fig. 2C), is 1.52 eV, 1.54 eV, and 1.55 eV for additive-free, $\text{M}\text{A}\text{C}\text{l}$ -, and $\text{M}\text{A}\text{C}\text{l}/\text{CsCl}$ -perovskite films, respectively. The slight variation in bandgap reflects the fine-tuning of the material properties due to the additives, further validating the improvements in efficiency. The normalized steady-state PL (Fig. 2D) also shows a blue shift for $\text{M}\text{A}\text{C}\text{l}$ - and $\text{M}\text{A}\text{C}\text{l}/\text{CsCl}$ -perovskite films, centering at 804 nm and 802 nm, respectively, as compared to the additive-free film (822 nm). This shift highlights the suppression of non-radiative recombination and supports the earlier claims of reduced defect density, improved carrier dynamics, and superior overall material quality when using dual additives.³²

The morphology and chemical composition of the $^{12}\text{C}\text{N}\text{P}/\text{C}\text{Q}\text{D}$ were analyzed using SEM, TEM, XRD, and Raman spectroscopy (Fig. S3, ESI[†]). Due to the unshielded environment, all analyses—except for performance verification—were conducted using normal citric acid ($^{12}\text{C}\text{A}$), adhering to international safety regulations for handling nuclear materials (Table S1, ESI[†]).

Furthermore, the electrochemical J - V characteristics of the PBC were evaluated and compared to control cells, optimized for perovskite film and the $^{14}\text{C}\text{N}\text{P}/\text{C}\text{Q}\text{D}$ electrode. The photovoltaic measurements demonstrated the J - V characteristics of both the $^{12}\text{C}\text{N}\text{P}/\text{C}\text{Q}\text{D}$ -based PBC and the Au-based control device (Fig. S4, ESI[†]). Statistical data, including open-circuit voltage (V_{oc}), short-circuit current density (J_{sc}), maximum power density (P_{max}), fill factor, and ECE, are provided in Table S2 (ESI[†]), showing that all samples performed reliably. Fig. 3A presents the J - V curve of betavoltaic perovskite cells using the radioactive isotope carbon-14 (^{14}C , 4.5 μCi). These cells operated with J_{sc} values of 30.36, 15.20, and 15.01 nA cm^{-2} , V_{oc} values of 0.01, 0.94, and 2.75 mV, and ECEs of 0.07%, 0.83%, and 1.83%, respectively. The dark characteristics of the cell, without C-14, were also measured (Fig. S5, ESI[†]).

The energy conversion efficiency of β -radiation was calculated using eqn (1),^{4,33}

$$\eta = \frac{P_{\text{max}}}{P_{\text{source}}} \times 100\% \quad (1)$$

$$= \frac{J_{\text{sc}} \times V_{\text{oc}} \times \text{FF}}{(3.7 \times 10^7) \times \phi \times E_{\text{avg}} \times e \times A} \times 100\%$$

Compared to the FAPbI_3 and $\text{M}\text{A}\text{C}\text{l}-\text{FAPbI}_3$ PBC, the $\text{M}\text{A}\text{C}\text{l}/\text{CsCl}-\text{FAPbI}_3$ PBC demonstrates superior betavoltaic performance. To further understand the interaction of β -particles with the perovskite absorber layer, Monte Carlo simulations were performed to estimate the energy deposition profile (Fig. S6, ESI[†]). The simulations revealed differences in the energy deposition profiles of β -particles within the perovskite ($\text{M}\text{A}\text{C}\text{l}/\text{CsCl}$ dual additive $\text{F}\text{a}\text{PbI}_3$ and $\text{F}\text{a}\text{PbI}_3$ only) and hole transport layer (HTL). The fluctuations in key variables, such as J_{sc} and V_{oc} , were largely attributed to variations in the β -electron emission rate.⁵ This enhanced performance is due to the dual additives, $\text{M}\text{A}\text{C}\text{l}$ and CsCl , which contribute to a highly crystalline structure and reduced defect density in the α -phase FAPbI_3 . The incorporation of these additives improves carrier dynamics, thus reducing recombination losses and enhancing efficiency. As a result, the $\text{M}\text{A}\text{C}\text{l}/\text{CsCl}$ -based PBC achieved a P_{max} of 0.024 nW cm^{-2} , Fig. 3B. Remarkably, the $\text{M}\text{A}\text{C}\text{l}/\text{CsCl}-\text{FAPbI}_3$ PBC generates 5.6×10^5 times more mobile electrons than the initial number of β -electrons. This indicates that excitons within the perovskite interact, leading to the formation of additional excitons or more free carriers when impacted by β -electrons. Hence, the excitons formed either interact to create additional excitons or release more free carriers (holes and electrons) when subjected to β -electrons. This synergistic behaviour indicates the material's potential for effective energy conversion.

To further explore this performance, we assessed the stability of the $\text{M}\text{A}\text{C}\text{l}/\text{CsCl}-\text{FAPbI}_3$ PBC by analyzing the variations in J_{sc} , V_{oc} , and ECE over time, as shown in Fig. 3C and D. The stability of these parameters is crucial for long-term operation. Fig. 3C demonstrates that the V_{oc} remained relatively stable at $2 \pm 1 \text{ mV}$, while J_{sc} was initially maintained at a minimum of 10 nA cm^{-2} , though it showed a gradual decline as time progressed. Despite this decrease, the PBC was able to sustain an ECE of approximately $1.8 \pm 0.2\%$ for up to 9 hours of continuous operation, which is a promising indicator of the device's operational stability. During this time, the device also maintained a stable PCE of approximately $1.5 \pm 0.2\%$, as shown in Fig. 3D. Following this period, a reduction in ECE was observed, likely due to surface damage caused by the continuous bombardment of β -electrons from the radioactive isotope source.¹⁰ Additionally, phase transitions from the desired α -phase into less favorable phases (δ -phase and PbI_2) at room temperature further contributed to this decline.³⁴ The overall ECE of the device is about 1.83%, which is reported for the first time in the world. While radiation-induced damage and phase instability play a role, exposure to moisture during both the fabrication process and operation is another key factor in the reduced efficiency. These findings highlight the importance of improving long-term material stability to ensure sustained device performance. However, we believe that the perovskite based betavoltaic device has the potential to achieve the expected efficiency of 28%, comparable to that of a solar cell. As this

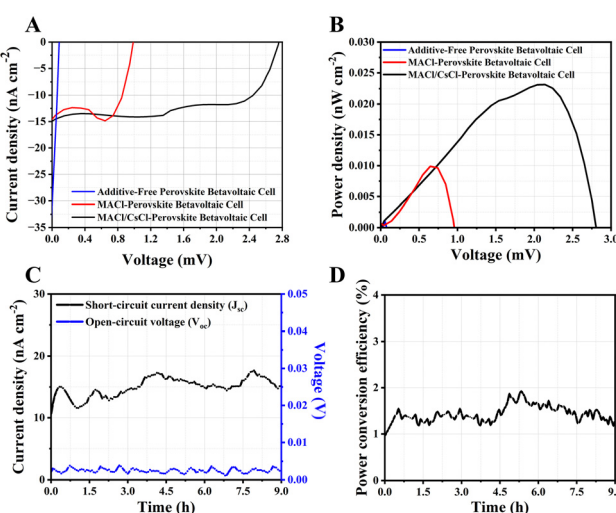


Fig. 3 Betavoltaic performance of FAPbI_3 -based perovskite cells: (A) J - V curve, and (B) P - V curve. Stability of the perovskite betavoltaic cell: (C) J_{sc} and V_{oc} , and (D) ECE.



is the first report of a betavoltaic cell directly integrated with perovskite, there remains substantial room for improvement. Nevertheless, compared to existing devices, the FAPbI_3 -based perovskite betavoltaic cell demonstrated the highest power density per radioactive source at $5.32 \text{ nW cm}^{-2} \text{ mCi}^{-1}$ (Tables S3 and S4, ESI[†]). Through collaborative efforts and further research, the aforementioned challenges can be overcome as the potential for perovskite in betavoltaic applications shows great promise.

In conclusion, this study successfully fabricated and demonstrated the high performance and stability of a FAPbI_3 -based perovskite betavoltaic cells using a dual additive strategy. By optimizing the ratio of MnCl and CsCl additives, we were able to enhance the crystallinity and reduce the defect density of the FAPbI_3 perovskite, as confirmed through comprehensive analysis of the material's morphology, crystallinity, and optoelectronic properties. The $\text{MnCl}/\text{CsCl}-\text{FAPbI}_3$ PBC achieved impressive parameters, including a J_{sc} of 15.01 nA cm^{-2} , a V_{oc} of 2.75 mV , and an ECE of 1.83% , all of which represent significant improvements over previous works. Compared to other betavoltaic cells reported in the literature, our PBC demonstrates the highest power density per radioactive source to date, positioning it as a potential breakthrough in nuclear battery technology. These results mark a considerable advancement in the field and provide a promising pathway toward the practical application of perovskite betavoltaic cells for energy generation in harsh environments where long-term, stable power is critical.

The authors acknowledge financial support from the Ministry of Science and ICT in Korea (2021R1A2C2009459) along with the support provided by the DGIST R&D program of the Ministry of Science and ICT of KOREA (24-N-HRHR-01).

Data availability

The data supporting this article have been included as part of the ESI.[†]

Conflicts of interest

There are no conflicts to declare.

Notes and references

- 1 M. Li, Y. Lu and X. Xu, *Environ. Sci. Pollut. Res.*, 2022, **29**, 64832–64845.
- 2 M. K. Singla, D. P. Nijhawan and D. A. S. Oberoi, *Int. J. Eng. Adv. Technol.*, 2019, **9**, 861–867.
- 3 M. B. Naseem, J. Lee and S.-I. In, *Chem. Commun.*, 2024, **60**, 14155–14167.

- 4 Y. Hwang, Y. H. Park, H. S. Kim, D. H. Kim, S. Ali, S. Sorcar, M. C. Flores, M. R. Hoffmann and S.-I. In, *Chem. Commun.*, 2020, **56**, 7080–7083.
- 5 H. S. Kim, J. Lee, S. Lee, N. S. Powar, M. B. Naseem, C. H. Kim, H. Zhou, H. K. Kim, W. A. Goddard and S.-I. In, *J. Power Sources*, 2024, **606**, 234427.
- 6 A. V. Sachenko, A. I. Shkrebtii, R. M. Korkishko, V. P. Kostylov, M. R. Kulish and I. O. Sokolovskyi, *Solid-State Electron.*, 2015, **111**, 147–152.
- 7 T. Shimaoka, H. Umezawa, K. Ichikawa, J. Pernot and S. Koizumi, *Appl. Phys. Lett.*, 2020, **117**, 103902.
- 8 H. San, S. Yao, X. Wang, Z. Cheng and X. Chen, *Appl. Radiat. Isot.*, 2013, **80**, 17–22.
- 9 Z. Ding, T.-X. Jiang, R.-R. Zheng, N. Wang, L.-F. Zhang, S.-C. Liu, X. Li and H.-S. San, *Nucl. Sci. Tech.*, 2022, **33**, 1–12.
- 10 M. B. Naseem, H. S. Kim, J. Lee, C. H. Kim and S.-I. In, *J. Phys. Chem. C*, 2023, **127**, 7565–7579.
- 11 N. Wang, Y. Ma, J. Chen, C. Chen, H. San, J. Chen and Z. Cheng, *Nanoscale*, 2018, **10**, 13028–13036.
- 12 J. Park, J. Kim, H.-S. Yun, M. J. Paik, E. Noh, H. J. Mun, M. G. Kim, T. J. Shin and S. I. Seok, *Nature*, 2023, **616**, 724–730.
- 13 G. Xing, N. Mathews, S. S. Lim, N. Yantara, X. Liu, D. Sabba, M. Grätzel, S. Mhaisalkar and T. C. Sum, *Nat. Mater.*, 2014, **13**, 476–480.
- 14 Z. Song, C. Zhao, F. Liao and Y. Zhao, *ACS Appl. Mater. Interfaces*, 2019, **11**, 32969–32977.
- 15 H. Nikjoo, S. Uehara and D. Emfietzoglou, *Interaction of Radiation with Matter*, CRC Press, 2016.
- 16 I. Pshenichnov, I. Mishustin and W. Greiner, *Nucl. Instrum. Methods Phys. Res., Sect. B*, 2008, **266**, 1094–1098.
- 17 S. Chen, X. Zhang, J. Zhao, Y. Zhang, G. Kong, Q. Li, N. Li, Y. Yu, N. Xu, J. Zhang, K. Liu, Q. Zhao, J. Cao, J. Feng, X. Li, J. Qi, D. Yu, J. Li and P. Gao, *Nat. Commun.*, 2018, **9**, 4807.
- 18 C. C. Boyd, R. Cheacharoen, T. Leijtens and M. D. McGehee, *Chem. Rev.*, 2019, **119**, 3418–3451.
- 19 I. S. Yang and N. Park, *Adv. Funct. Mater.*, 2021, **31**, 2100396.
- 20 D.-H. Kang, S.-U. Lee and N.-G. Park, *ACS Energy Lett.*, 2023, **8**, 2122–2129.
- 21 P. Wang, Q. Jiang, Y. Zhao, Y. Chen, Z. Chu, X. Zhang, Y. Zhou and J. You, *Sci. Bull.*, 2018, **63**, 726–731.
- 22 W. Li, J. Li, G. Niu and L. Wang, *J. Mater. Chem. A*, 2016, **4**, 11688–11695.
- 23 D.-K. Lee and N.-G. Park, *Appl. Phys. Rev.*, 2023, **10**(1), 011308.
- 24 L. McGovern, M. H. Futscher, L. A. Muscarella and B. Ehrler, *J. Phys. Chem. Lett.*, 2020, **11**, 7127–7132.
- 25 G. Li, C. Zhao, Y. Liu, J. Ren, Z. Zhang, H. Di, W. Jiang, J. Mei and Y. Zhao, *ACS Omega*, 2021, **6**, 20015–20025.
- 26 S. Prathapani, D. Choudhary, S. Mallick, P. Bhargava and A. Yella, *CrystEngComm*, 2017, **19**, 3834–3843.
- 27 Y. Guo, S. Yuan, D. Zhu, M. Yu, H.-Y. Wang, J. Lin, Y. Wang, Y. Qin, J.-P. Zhang and X.-C. Ai, *Phys. Chem. Chem. Phys.*, 2021, **23**, 6162–6170.
- 28 H. Wang, M. Hao, J. Han, M. Yu, Y. Qin, P. Zhang, Z. Guo, X. Ai and J. Zhang, *Chem. – Eur. J.*, 2017, **23**, 3986–3992.
- 29 G. Kim, C. S. Moon, T.-Y. Yang, Y. Y. Kim, J. Chung, E. H. Jung, T. J. Shin, N. J. Jeon, H. H. Park and J. Seo, *Sol. RRL*, 2020, **4**(6), 2000033.
- 30 Y. Chen, Q. Meng, Y. Xiao, X. Zhang, J. Sun, C. B. Han, H. Gao, Y. Zhang, Y. Lu and H. Yan, *ACS Appl. Mater. Interfaces*, 2019, **11**, 44101–44108.
- 31 M. Wang, Y. Lu, X. Huo, Q. Cai, Y. Yao, Y. Zhang, D. Song, Z. Xu, S. Chen, G. Chen, X. Li and D. Wei, *J. Power Sources*, 2023, **561**, 232753.
- 32 I. S. Jin, K. S. Kim and J. W. Jung, *J. Power Sources*, 2021, **512**, 230481.
- 33 T. Wacharasindhu, J. W. Kwon, D. E. Meier and J. D. Robertson, *Appl. Phys. Lett.*, 2009, **95**(1), 014103.
- 34 Q. Han, S. Bae, P. Sun, Y. Hsieh, Y. (Micheal) Yang, Y. S. Rim, H. Zhao, Q. Chen, W. Shi, G. Li and Y. Yang, *Adv. Mater.*, 2016, **28**(11), 2253–2258.

